Available online at www.sciencedirect.com
ScienceDirect
Journal of Inorganic Biochemistry xxx (2008) xxx–xxx
JOURNAL OF Inorganic Biochemistry
www.elsevier.com/locate/jinorgbio

Theoretical insight into the hydroxylamine oxidoreductase mechanism

M. Laura Fernández, Darío A. Estrin *, Sara E. Bari *

Departamento de Química Inorgánica, Analítica y Química Física/INQUIMAE-CONICET, Facultad de Ciencias Exactas y Naturales, Universidad de Buenos Aires, Ciudad Universitaria, Pabellón 2, Buenos Aires, C1428EHA, Argentina

Received 16 August 2007; received in revised form 18 January 2008

Abstract

The multiheme enzyme hydroxylamine oxidoreductase from the autotrophic bacteria *Nitrosomonas europaea* catalyzes the conversion of hydroxylamine to nitrite, with a complicate arrangement of heme groups in three subunits. As a distinctive feature, the protein has a covalent linkage between a tyrosyl residue of one subunit and a *meso* carbon atom of the heme active site of another. We studied the influence of this bond in the catalysis from a theoretical perspective through electronic structure calculations at the density functional theory level, starting from the crystal structure of the protein. Geometry optimizations of proposed reaction intermediates were used to calculate the dissociation energy of different nitrogen containing ligands, considering the presence and absence of the *meso* tyrosyl residue. The results indicate that the tyrosine residue enhances the binding of hydroxylamine, and increases the stability of a $Fe^{III}NO$ intermediate, while behaving indifferently in the $Fe^{II}NO$ form. The calculations performed on model systems including neighboring aminoacids revealed the probable formation of a bidentate hydrogen bond between the $Fe^{III}H_2O$ complex and Asp 257, in a high-spin aquo complex as the resting state. Characterization of non-planar heme distortions showed that the *meso*-substituent induces significant ruffling in the evaluated intermediates.

Keywords: Hydroxylamine oxidoreductase; Catalytic activity; *meso*-Substituted heme; DFT

1. Introduction

Hydroxylamine (NH_2OH) is a natural product found in mammalian cells and bacteria. In the former, NH_2OH may be formed from decomposition of nitrosothiols [1]. In bacteria, it is related to the nitrogen cycle as starting material for nitrite and ammonia formation or as a critical intermediate in their interconversion [2,3]. The catalytic disproportionation of NH_2OH is known to be mediated by hemoglobin, forming equal amounts of ammonia (NH_3) and nitrous oxide (N_2O) [4–6], by myoglobin [7], and also by non-heme transition metal complexes, where the distribution of nitrogen products depends on the metal, the ligands, the pH, and the reaction medium [8,9].

With a complicated arrangement of heme groups, the multiheme enzyme hydroxylamine oxidoreductase (HAO) from the autotrophic bacteria *Nitrosomonas europaea*, catalyzes the two step conversion of NH_2OH to nitrite (NO_2^-) [10]. It was purified to homogeneity more than 20 years ago and its crystal structure at 2.8 Å resolution has been published [11]. It is one of the most complex heme containing enzymes known to date. The distinctive feature of this periplasmic protein is that it has three subunits [12] linked with each other through a covalent bond between a C3 of a tyrosyl residue of one subunit and a 5-*meso* carbon atom of *c*-type heme of another, to form a homotrimer shaped like a garlic head with a total of 24 heme groups [11,13]. The linker *meso*-substituted heme group is called P_{460}, due to the absorbance of the ferrous form; the other seven hemes per subunit are common *c*-type hemes.

* Corresponding authors. Tel.: +54 11 45763300x236; fax: +54 11 45763341 (S.E. Bari), tel.: +54 11 45763378x105; fax: +54 11 45763341 (D.A. Estrin).
E-mail addresses: dario@qi.fcen.uba.ar (D.A. Estrin), bari@qi.fcen.uba.ar (S.E. Bari).

0162-0134/$ - see front matter © 2008 Elsevier Inc. All rights reserved.
doi:10.1016/j.jinorgbio.2008.01.032

The iron atom of the P_{460} heme has been described as pentacoordinated (5c) in the ferric state with a vacant coordination site available for the substrate, though seemingly exposed to solvent ligation [11]. By combination of Mössbauer and EPR spectroscopies, pioneering studies suggested that the heme active site in the fully oxidized HAO could be in a high-spin (hs) state [14–17]. The other *c*-type hemes are in the low-spin (ls) ferric state, hexacoordinated (6c) to two histidines each, forming an extraordinarily optimized electron transfer chain [18,19].

The energy derived from the overall process is critical for bacterial growth and consequently of enormous ecological and economic relevance. Special focus has been placed on the electron transfer process and the electrostatic influence of neighboring heme groups. Particularly, theoretical calculations and careful experimental measurements suggested that the difference between the redox potential of the solvent exposed heme P_{460} and heme 2 results in retention of the electrons generated in the oxidation of NH_2OH, and they are only injected into the electron transfer chain when cytochrome c554, HAO's physiological electron transfer partner, is attached to HAO shifting P_{460} potential to a more positive value [19].

The nitrogen containing intermediates of the catalytic conversion of NH_2OH to NO_2^- are subject of active debate, particularly the formation of the $Fe^{III}NO/Fe^{II}NO^+$ and $Fe^{II}NO$ P_{460} complexes ($\{FeNO\}^6$ and $\{FeNO\}^7$ respectively, according to the Enemark–Feltham notation [21]). Hendrich and co-workers showed that the reaction of fully oxidized HAO with 1 atm of nitric oxide (NO), yields a surprisingly stable $\{FeNO\}^6$ species (K_{eq} aprox. $10^5\ M^{-1}$ or higher) [22]. In the same direction, Cabail and co-workers obtained an equilibrium binding constant for the net nitrosylation reaction, $K_{eq} = (7.7 \pm 0.6) \times 10^4\ M^{-1}$ [23,24], a value about five times greater than that obtained for metmyoglobin or methemoglobin, but orders of magnitude smaller than the corresponding K_{eq} for ferrous hemeproteins ($10^{11}\ M^{-1}$) [25,26]. In general, the ferric hemeproteins exhibit fast dissociation rates for NO (k_{diss}=0.65 to 40 s^{-1}) leading to small binding constants $K_{eq} = 10^3$–$10^5\ M^{-1}$, while nitrosyl ferrous hemeproteins show slow dissociation rates ($k_{diss} = 4 \times 10^{-4}\ s^{-1}$), and consequently large $K_{eq} = 10^{11}$–$10^{12}\ M^{-1}$ [27–29]. The presence of a stable $\{FeNO\}^6$ moiety in proteins finds a precedent in nitrophorins, where the stability of the $\{FeNO\}^6$ form is attributed to a pH-dependent conformational change that traps the NO in the active site, and to a ruffled conformation of the heme active site [30–32].

Non-planar distortions of heme prosthetic groups exert a direct influence in the catalytic activity of the hemeproteins. As a very general starting point, the asymmetric pattern of β substitution of the majority of porphyrin cofactors in natural compounds (protoporphyrin IX, chlorophyll or bacteriochlorophyll derivatives) is capable of mild out-of-plane deviations in the porphyrin macrocycle (aprox. 0.5 Å) [33]. More dramatically, the effect of metal coordination, non covalent and covalent bonds to aminoacid residues, and the conformational constraints imposed by the different apoproteins result in stronger non-planar, mixed-mode deviations. Such deviations explain the wide spectra of catalytic reactions and physicochemical processes that can be performed by the same prosthetic group [34–36]. In the last 20 years *meso*-substituted synthetic porphyrins and metalloporphyrins have been extensively used to study the relationship between planarity deviations, physicochemi-

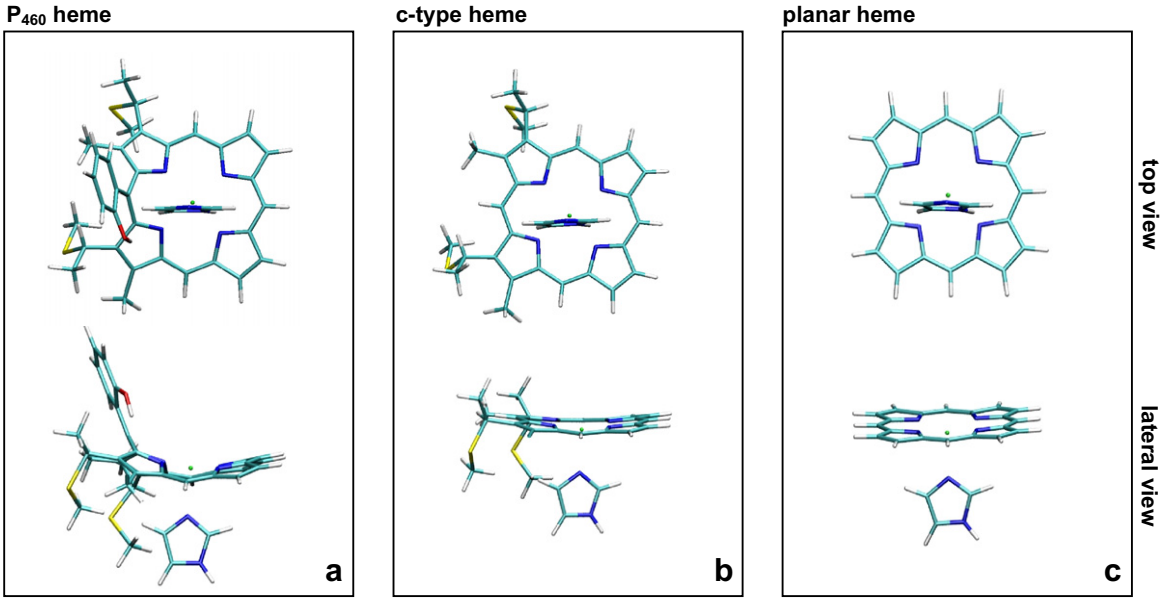

Fig. 1. Optimized structures of the model systems.

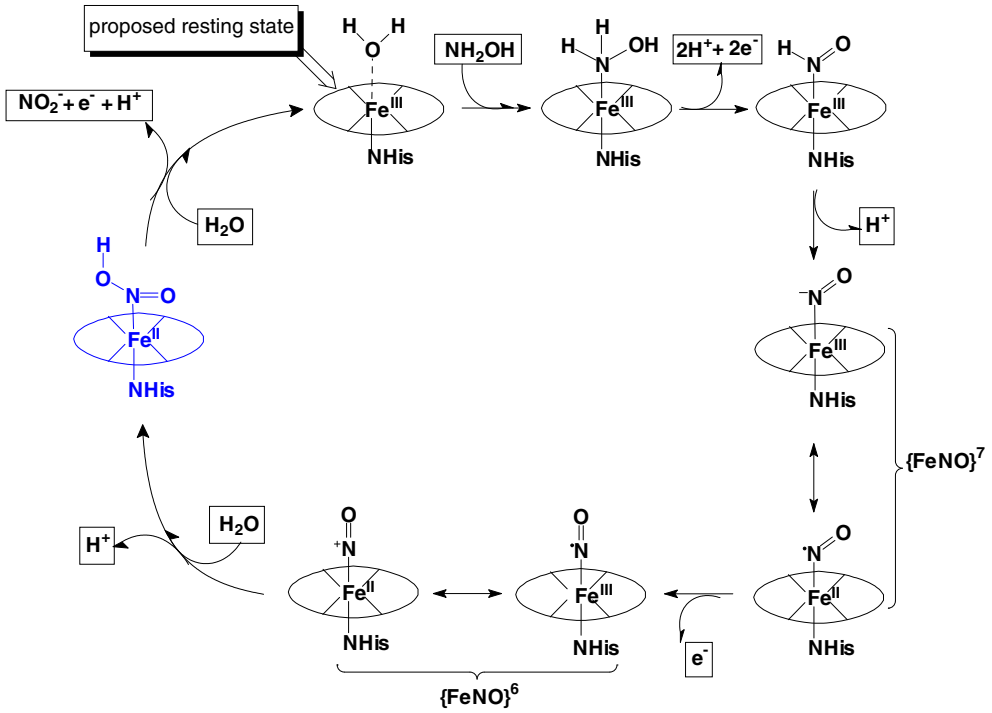

Fig. 2. Putative N-containing intermediates at the P_{460} active site of hydroxylamine oxidoreductase in the conversion of NH_2OH into NO_2^-.

cal properties and chemical reactivity. Aside from the P_{460} in HAO, mono *meso*-substitution has only been found in nature in cytochrome P_{460} of *N. europaea*, as a crosslink between a c-type heme and a lysine residue [37–39,20].

Focusing on the binding site, we performed quantum computations on three model systems (the P_{460} heme, a c-type heme and a planar iron porphine) in order to analyze the influence of the covalent *meso*-substituent and the non-planar heme deviations on the catalytic reaction (Fig. 1). The metal–ligand binding energy, the differences in charge distribution and in geometrical parameters of Fe^{III}—NH_2OH, Fe^{III}—HNO, $\{FeNO\}^7$, $\{FeNO\}^6$, which are the currently accepted reaction intermediates [24], were calculated for the hypothetical scenarios, to determine the influence of the *meso*-substituent on the conversion of NH_2OH to NO_2^- (Fig. 2). Computations on extended model systems provided a deeper insight into the participation of relevant aminoacids of the active site (Asp 257, His 258, Tyr 334), both on the spin state of the resting form and on the specific characterization of the coordination status on the catalytic activity of heme P_{460}. To improve the description of the system from this theoretical point of view, we considered the absence or presence of a water molecule as a sixth ligand in the resting form (hs, pentacoordinated Fe^{III} or hs, Fe^{III}—H_2O, respectively), a feature that could not be unequivocally deduced from the crystal structure. Calculations on extended model systems were also applied to the study of the participation of the tyrosyl residue in the putative

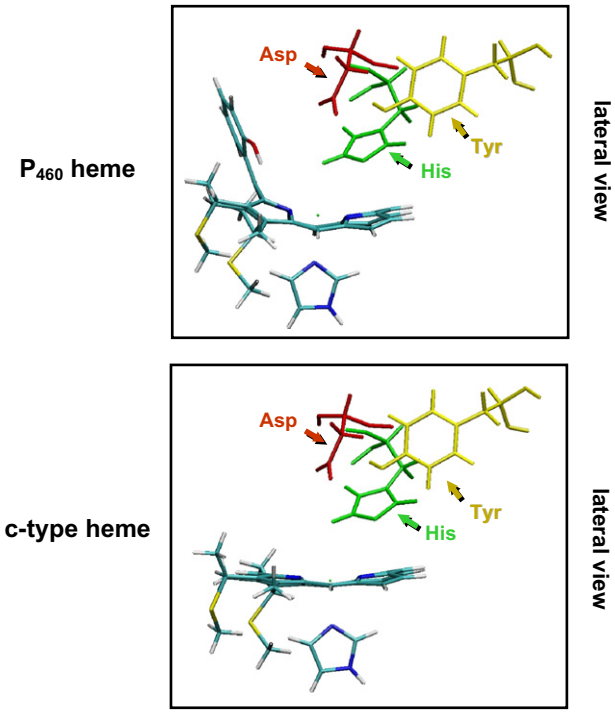

Fig. 3. Optimized structures of the extended model systems.

last steps of the catalytic process: $\{FeNO\}^6$ in the presence of the aminoacidic environment, its hydration to Fe^{II}—HNO_2, and the final formation and cleavage of the product NO_2^- (Figs. 2 and 3).

2. Experimental

2.1. Model systems and computational methods

The initial structure representing the HAO active site was constructed from a theoretical 3D structure obtained from the crystallographic data[1] (pdb code: 1FGJ) [11].

2.1.1. Heme model systems

Fig. 1 depicts the three heme model systems designed for the calculations: P_{460} model (Fig. 1a), c-type heme model (Fig. 1b) and Fe-porphine model (Fig. 1c). The proximal histidine of the heme active site was introduced as an imidazole. In the P_{460} and c-type heme model systems, both propionate side chains and methyl substituents were replaced by hydrogens, and the covalent bonds to cysteine residues were simplified as methylthioether groups. In the P_{460} model system, the covalent *meso*-linked tyrosyl residue was represented by an *o*-phenyl residue.

Extended model systems, including a classical description of relevant aminoacids (Asp 257, His 258 and Tyr 334) of the active site, were optimized to shed light on their direct participation on the description of the catalytic activity (Fig. 3).

The conversion of NH_2OH to NO_2^-, was analyzed in these models from a theoretical perspective considering reaction intermediates proposed on the basis of previous literature [3,24] (Fig. 2).

2.1.2. Computational methods

All the calculations were performed *in vacuo*. Calculations for the heme model systems were performed at the DFT level, using the SIESTA code as described previously [40,41]. Briefly, the SIESTA method uses standard norm-conserving pseudopotentials [42], to avoid the computation of core electrons, while simultaneously smoothing the valence charge density. Also a nonlinear partial-core correction was applied to iron [43]. The generalized gradient approximation functional proposed by Perdew et al. [44], already validated for heme models [45,46], was used to perform the calculations. Investigation of heme systems using DFT yielded reasonable results for structural parameters, and greatly contributed to the interpretation and understanding of the functional aspects of the active site of hemoproteins at the molecular level. However, attempts to predict the ground state multiplicity of these systems soon made apparent that an accurate description of the spin state might require more sophisticated techniques [47]. This fact can be tracked down to the fact that it has been systematically observed that Hartree-Fock favors high-spin electronic configurations while DFT exhibits a preference for low-spin states [48,49]. These well known DFT flaws, however, are not expected to affect the comparative analysis performed in this work between different P_{460} model systems.

The geometry optimizations for the extended model systems (Fig. 3) were performed using a conjugate gradient scheme and a hybrid approach in which the ligand, the heme, and the proximal aminoacid were treated quantum mechanically, and the distal aminoacids were described using the Amber 99 force field parametrization [50]. Restricted optimizations for the residues Asp 257, His 258 and Tyr 334 were performed by anchoring points to their original position within the protein crystallographic structure.

Effects of the zero-point energies were neglected throughout. This choice was motivated by the fact that, in many cases, we were interested in computing binding energies from single point calculations at selected non-minimum structures, for which this kind of computations is not possible. Basis set superposition errors were not considered, since these errors are supposed to cancel in the comparisons performed.

2.1.3. Calculations

The calculations on the pentacoordinated (5c) ferrous heme model system were performed on the high-spin multiplicity, the experimental spin state of the fully reduced HAO [16]. The 5c ferric heme model systems, as putative resting forms, were calculated as high-spin states [11]. All the ferric reaction intermediates (hexacoordinated nitrogen containing ligands) were modeled in the low-spin multiplicity. The hexacoordinated (6c), aquo ferric complexes, as alternative resting forms, were modeled in the high and low-spin states (see below).

The Fe-ligand dissociation energies (ΔE_L) for the ferrous intermediates were calculated as:

$$\Delta E_L = (E_{Fe\text{–}His} + E_L) - E_{His\text{–}Fe\text{–}L}$$

The Fe-ligand dissociation energies (ΔE_L) for the ferric intermediates were computed considering three possible resting forms:

1. Pentacoordinated, high-spin resting form:

$$\Delta E_L = (E_{Fe\text{–}His} + E_L) - E_{His\text{–}Fe\text{–}L}$$

2. Hexacoordinated, high/low-spin aquo complex as the resting form:

$$\Delta E_L = (E_{His\text{–}Fe\text{–}H_2O} + E_L) - (E_{His\text{–}Fe\text{–}L} - E_{H_2O})$$

For each model system, $E_{Fe\text{–}His}$ is the energy of 5c, high-spin porphyrin-imidazole complex, E_L are the energies of the isolated ligands ($L = NH_2OH$, HNO, NO, HNO_2, NO_2^-), and $E_{His\text{–}Fe\text{–}L}$ is the energy obtained for each 6c, low-spin complex. $E_{His\text{–}Fe\text{–}H2O}$ is the energy obtained for the 6c, high-spin or low-spin aquo complexes, and E_{H2O} is the energy of a H_2O isolated molecule.

2.1.4. Heme geometric distortions

Characterization of the heme distortions (saddling, ruffling, doming, waving [wav(x), wav(y)] and propellering)

[1] The predicted tridimensional structure of the homotrimer (subunit 0, 1 and 2) was sent to us by Dr. Igarashi and Dr. Tanaka, as the crystals isolated were composed by two independent subunits.

for all model systems was obtained using the normal-coordinate structural decomposition (NSD) method [34].

2.1.5. Single point analysis

The optimized geometry of each intermediate of the catalytic process derived from the P_{460} model system was used to calculate the energy in a single point after the replacement of the tyrosyl residue by a hydrogen atom. The Fe-Ligand dissociation energies (ΔE_L) were calculated as:

1. Pentacoordinated, high-spin resting form:

$$\Delta E_L = (E_{Fe\text{–}His(SP)} + E_L) - E_{His\text{–}Fe\text{–}L(SP)}$$

2. Hexacoordinated, high/low-spin aquo complex as the resting form:

$$\Delta E_L = (E_{His\text{–}Fe\text{–}H_2O(SP)} + E_L) - (E_{His\text{–}Fe\text{–}L(SP)} - E_{H_2O})$$

3. Results and discussion

3.1. Heme-Ligand dissociation energies in the heme model systems

The resting state of HAO has been previously described as pentacoordinated from the 2.8 Å crystal structure [11], with a significant exposure to the water environment. The spin state of the resting form of HAO has not been unequivocally assessed yet [14,16,52]. Accordingly, in our calculations the resting state was considered as 5c, high-spin or as a 6c, high or low-spin aquo complex. The 6c, ls aquo complex showed that the calculated distance Fe—H_2O was identical in the presence or absence of the tyrosyl residue (2.07 Å), while in the 6c, hs aquo complex were 2.41 Å and 2.40 Å, respectively. This observation suggested that the longer Fe—H_2O bond could enable a stabilizing hydrogen bond (H-bond) to proximal aminoacids. Calculations including a classical description of three relevant neighboring aminoacids provided a deeper insight into this issue. This configuration was previously described for metmyoglobin, where a hs aquo complex was favored by stabilization with a proximal histidine [53,54].

The binding of the substrate NH_2OH was found to be enhanced in the presence of the tyrosyl residue only when calculations were performed on the 6c, hs aquo configurations. Thus we considered the 6c, hs or the 5c, hs forms of the resting state to evaluate the effect of the presence or absence of the tyrosyl residue.

The *meso*-covalent linked tyrosyl residue enhanced the binding of the natural substrate hydroxylamine by 9.3 kcal/mol considering the 5c, hs resting form and by 7.2 kcal/mol for the 6c, hs aquo as the resting form (Table 1). The presence of the *meso*-substituent also enhanced the stability of the Fe^{III}—HNO and the $\{FeNO\}^6$ intermediates (13.0 and 8.4 kcal/mol, and 10.7 and 6.2 kcal/mol for the hs 5c- and 6c-resting forms, respectively). On the contrary, *meso*-substitution was seen to behave indifferently in the $\{FeNO\}^7$ intermediate, suggesting a strategy against the autoinhibition of the enzyme by a highly stable $\{FeNO\}^7$ form. The comparison with the minimal and planar iron porphine provided an adequate reference to our calculations.

Table 1
Dissociation energies for the catalysis intermediates proposed for HAO activity[a]

Heme model	ΔE_{LIGAND}[b]			ΔE_{LIGAND}[c]		
	P_{460}	c-Type	Planar	P_{460}	c-Type	Planar
Fe^{III}—NH_2OH	−42.5	−33.2	−33.0	−33.4	−26.2	−26.0
Fe^{III}—HNO	−55.9	−42.9	−41.7	−46.7	−36.0	−34.7
$\{FeNO\}^6$	−56.1	−47.7	−49.2	−46.9	−40.7	−42.2
$\{FeNO\}^7$	−50.4	−48.8	−50.1			

[a] Energies in kcal/mol.
[b] Vs. pentacoordinated, high-spin resting form.
[c] Vs. hexacoordinated, high-spin resting form.

3.2. Heme-ligand dissociation energies in the extended model systems

Calculations on the extended model systems showed a relevant interaction, specifically a bidentate hydrogen bond between Asp 257 and the coordinated water molecule, supporting the presence of a 6c, hs aquo complex as the resting state (Fig. 4). This result can be regarded as a new starting point to the theoretical study of the hydroxylamine oxidoreductase. As an additional effect, the Asp 257 residue critically constrained the orientation of the natural substrate in our calculations (Fig. 4).

Table 2 shows the dissociation energies for the extended models, for the different proposed intermediate complexes. The natural substrate NH_2OH, and the intermediate ligands HNO and NO showed a significantly stronger Fe—N bond in the extended models, when considering the 5c, hs resting form, while the presence of the distal aminoacids did not show a relevant effect in the ferrous intermediate $\{FeNO\}^7$. Results are in good accordance with the calculations on the corresponding heme models, taking into account the incidence of a more stabilized resting state, traced to H-bonding stabilization.

Considering the 6c, hs aquo resting state, only the natural substrate followed a similar trend in the extended models and in the reduced ones. In fact, the calculations on the extended model systems for the Fe^{III}—HNO and $\{FeNO\}^6$ intermediates suggest lower dissociation energies, only reflecting the increased stabilization of the resting form.

The extended model systems were also used to calculate the dissociation energy for Fe^{II}—HNO_2 and Fe^{III}—NO_2^- in order to shed light on the last step of the catalytic cycle. Hydration followed by a one electron oxidation of the Fe^{II}—NO^+ intermediate promoted the lability of the desired product NO_2^-, and gave back the resting state for a new catalytic cycle. Table 2 shows that the tyrosyl residue in the P_{460} weakens the Fe^{II}—N bond for the HNO_2 ligand in comparison to the c-type heme (−33.5 vs. −37.3 kcal/

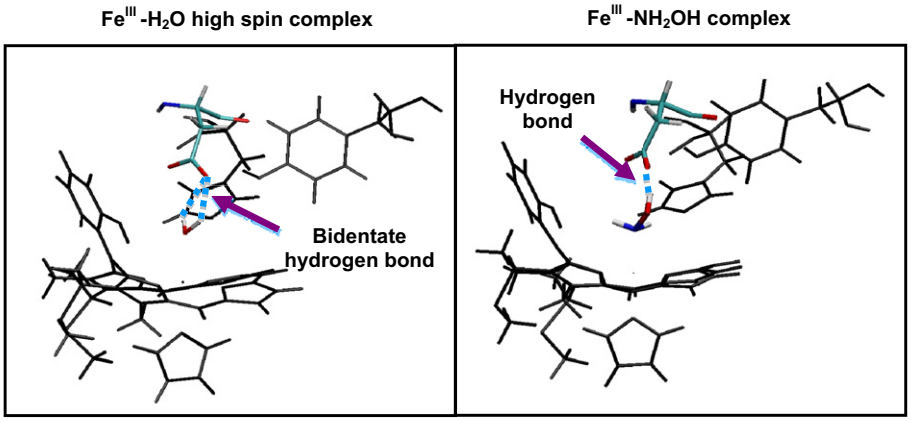

Fig. 4. H_2O or NH_2OH as sixth ligands of the binding site of HAO.

Table 2
Dissociation energies for the catalysis intermediates proposed for HAO activity in the extended model systems[a]

Heme model	ΔE_{LIGAND}[b]		ΔE_{LIGAND}[c]	
	P_{460}	c-Type	P_{460}	c-Type
Fe^{III}—NH_2OH	−74.3	−69.1	−42.4	−36.8
Fe^{III}—HNO	−73.5	−66.7	−41.3	−34.4
$\{FeNO\}^6$	−66.2	−61.8	−34.3	−29.3
$\{FeNO\}^7$	−51.9	−53.0	–	–
Fe^{II}—HNO_2	−33.5	−37.3	–	–
Fe^{III}—NO_2^-	−87.0	−94.9	−55.1	−54.8

[a] Energies in kcal/mol.
[b] Vs. pentacoordinated, high-spin resting form.
[c] Vs. hexacoordinated, high-spin resting form.

mol, respectively) in the extended models, exhibiting an opposite behavior in comparison to the other nitrogenated species considered in the catalytic cycle. Similar calculations for NO_2^-, suggest that the presence of the *meso*-substituent does not favour the binding of the desired reaction product.

According to Mülliken populations, the net charge on the NO moiety of the intermediate $\{FeNO\}^6$ adopts a higher positive value in the presence of the neighbouring aminoacids, implying the Fe^{II}—NO^+ resonance structure is favored ($qNO = 0.380$ and $qNO = 0.240$, for the extended and the isolated P_{460} model systems, respectively). The tyrosil residue does not exert a significant effect on the net charge on the NO moiety (data not shown).

3.3. Analysis of the heme distortion

Characterization of the non-planar heme distortions for the wild type (P_{460}), the heme without the covalent tyrosine-C3 bond (c-type heme), and a planar porphine were performed using the normal-coordinate structural decomposition procedure [34,51]. This method allowed to evaluate the displacements of our optimized model systems from the normal geometries, described by six out-of-plane normal deformations.

Table 3
Calculated total out-of plane distortions (Å)

Heme model	P_{460}	c-Type	Planar
Fe^{III}—NH_2OH	2.15	1.11	0.14
Fe^{III}—HNO	2.18	1.05	0.09
$\{FeNO\}^7$	1.93	0.84	0.08
$\{FeNO\}^6$	2.00	0.98	0.18

Table 3 shows that the tyrosyl residue induces a severe distortion in the heme model systems, and that the magnitude of the deformation is conserved in the intermediates evaluated. Previous research using crystallographic data indicates that macrocycle deformations of c-type hemes are characterized by highly ruffled macrocycles (total distortion ranging from 0.7 to 1.2 Å); the saddling and waving (x, y) deviation modes are also present to a lesser extent [55]. The magnitude of global distortion observed in the modeled P_{460}, ca. 2 Å, was observed previously in synthetic nickel porphyrins [34,56].

The combination of the ruffling and the *wav*(x) and *wav*(y) deformations resulted in an asymmetric ruffling distortion, where the *meso* carbon (C5) bound covalently to the tyrosyl residue of the heme active site was highly distorted in comparison with the other *meso* carbons, in good agreement with the observed trends on the ferrocytochrome c and its mutants [54]. The decomposition data obtained for our optimized models shown in Table 4 indicate that the *meso*-substitututed P_{460} model system is even more ruffled than the regular c-type hemes. Recent research based on the crystal structure of cytochrome P_{460} of *N. europaea* [20], where a lysine residue is covalently attached to a γ *meso* position of a heme group, indicates sp^3 hybridization at this cross-linking point. The calculated bond length C_α–C5 (C_α – α *meso*) in the optimized P_{460} model system is intermediate (1.46 Å) between the homologous in a porphodimethene structure ($d_{C\alpha-C5} = 1.50$ Å, sp^3-C5) [57] and in a c-heme moiety ($d_{C\alpha-C5} = 1.41$ Å), suggesting the possibility of conservation of the porphyrinic aromatic system even in this severely distorted macrocycle.

Table 4
Decomposition data for the optimized models (Å)

Heme model	P_{460}					c-Type					Planar				
Geometric distortion	Ruf.	Sad.	Dom.	Wav. (x)	Wav. (y)	Ruf.	Sad.	Dom.	Wav. (x)	Wav. (y)	Ruf.	Sad.	Dom.	Wav. (x)	Wav. (y)
Fe^{III}—NH_2OH	2.05	0.26	0.35	0.31	0.37	1.02	0.24	0.10	0.05	0.05	0.11	0.05	0.06	0.05	0.01
Fe^{III}—HNO	2.08	0.18	0.37	0.32	0.37	1.09	0.15	0.06	0.06	0.05	0.06	0.05	0.03	0.02	0.01
$\{FeNO\}^7$	1.79	0.34	0.34	0.41	0.31	0.83	0.03	0.12	0.05	0.05	0.02	0.04	0.05	0.02	0.02
$\{FeNO\}^6$	1.87	0.34	0.38	0.32	0.41	0.97	0.08	0.03	0.04	0.06	0.16	0.05	0.05	0.03	0.02

3.4. Single point determinations for NH_2OH and NO binding

The dissociation energies of NH_2OH and NO were calculated as previously stated (see above), but replacing the tyrosyl residue by a hydrogen atom in the highly distorted optimized structure of the P_{460}. These single point calculations allow discrimination between conformational and electronic effects induced by the *meso* tyrosyl residue. Table 5 shows that in both heme types the binding of the natural substrate and of the NO to the Fe^{III} form exhibit a dominating, stabilizing, conformational effect over a destabilizing electronic effect. The sole presence of the conformational effect of the tyrosyl residue did not significantly modify the binding of the NO to the oxidized form (−56.1 vs. −58.9 kcal/mol). On the contrary, the tyrosyl residue in the Fe^{II} state had a relevant negative electronic effect on the binding of NO; since its absence significantly enhaced the binding energy (−50.4 vs. −56.0 kcal/mol). The stability of the $\{FeNO\}^7$ form is particularly disfavoured by the tyrosyl residue, preventing its role as dead end in this distorted heme catalytic site and allowing the desired evolution of the catalytic reaction.

After deprotonation to its conjugate base, the Fe^{III}—HNO form has been postulated to yield the $\{FeNO\}^7$ complex. The presence of the tyrosyl residue revealed an active participation in the destabilization of this intermediate, both preventing a dead end for the catalytic cycle and enabling the oxidation to $\{FeNO\}^6$. The stability of this elusive complex is enhanced by the presence of the tyrosyl residue, and the highly ruffled conformation it induces. The enhanced stabilization of $\{FeNO\}^6$ forms induced by ruffling deformations finds a precedent in the nitrophorins [30–32].

Theoretical calculations suggest that the presence of the *meso* tyrosyl residue in the P_{460} active site of the HAO of *N. europaea* positively cooperates with the currently accepted catalytic cycle, on the basis of a 6c, hs aquo resting state as the starting point.

Table 5
Single point calculations for the binding of NH_2OH and NO

	ΔE_{LIGAND} [b]		ΔE_{LIGAND} [c]
Binding of NH_2OH [a]	Fe^{II}	Fe^{III}	Fe^{III}
P_{460} heme [d]	–	−42.5	−33.4
SP	–	−47.9	−37.3
c-type heme [d]	–	−33.2	−26.2
Binding of NO [a]			
P_{460} heme [d]	−50.4	−56.1	−46.9
SP	−56.0	−58.9	−48.3
c-type heme [d]	−48.8	−47.7	−40.7

[a] Energies in kcal/mol.
[b] Vs. pentacoordinated, high-spin resting form.
[c] Vs. hexacoordinated, high-spin resting form.
[d] Data from Table 1.

4. Abbreviations

DFT	density functional theory
HAO	hydroxylamine oxidoreductase
NSD	normal-coordinate structural decomposition
ls	low-spin
hs	high-spin
5c	pentacoordinated
6c	hexacoordinated

Acknowledgements

We thank Dr. Igarashi and Dr. Tanaka for providing the predicted tridimensional structure of the homotrimer of HAO. This work was supported by grants of CONICET, University of Buenos Aires, and ANPCyT. Authors are members of CONICET staff.

References

[1] P.S.Y. Wong, J. Hyun, J.M. Fukuto, F.N. Shirota, E.G. DeMaster, D.W. Shoeman, H.T. Nagasawa, Biochemistry 37 (1998) 5362–5371.
[2] J. Schalk, S. de Vries, J.G. Kuenen, M.S.M. Jetten, Biochemistry 39 (2000) 5405–5412.
[3] O.A. Einsle, A. Messerschmidt, R. Huber, P.M.H. Kroneck, F. Neese, J. Am. Chem. Soc. 124 (2002) 11737–11745.
[4] D.A. Bazylinski, R.A. Arkowitz, T.C. Hollocher, Arch. Biochem. Biophys. 259 (1987) 520–526.
[5] K. Stolze, H. Nohl, Biochem. Pharmacol. 38 (1989) 3055–3059.
[6] K. Stolze, A. Dadak, Y. Liu, H. Nohl, Biochem. Pharmacol. 52 (1996) 1821–1829.
[7] J. Taira, V. Misik, P. Riesz, Biochim. Biophys. Acta 1336 (1997) 502–508.
[8] S.K. Wolfe, C. Andrade, J.H. Swinehart, Inorg. Chem. 13 (1974) 2567–2572.
[9] G.E. Alluisetti, A.E. Almaraz, V.T. Amorebieta, F. Doctorovich, J.A. Olabe, J. Am. Chem. Soc. 126 (2004) 13431–13432.
[10] K.R. Terry, A.B. Hooper, Biochemistry 20 (1981) 7026–7032.
[11] N. Igarashi, H. Moriyama, Y. Fukuomori, N. Tanaka, Nat. Struct. Biol. 4 (1997) 276–284.
[12] D.M. Arciero, A.B. Hooper, J. Biol. Chem. 268 (1993) 14645–14654.
[13] D.M. Arciero, A.B. Hooper, M. Cai, R. Timkovich, Biochemistry 32 (1993) 9370–9378.
[14] J.D. Lipscomb, A.B. Hooper, Biochemistry 21 (1982) 3965–3972.
[15] J.D. Lipscomb, K.K. Andersson, E. Münck, T.A. Kent, A.B. Hooper, Biochemistry 21 (1982) 3973–3976.
[16] K.K. Andersson, T.A. Kent, J.D. Lipscomb, A.B. Hooper, E. Münck, J. Biol. Chem. 259 (1984) 6833–6840.
[17] D.M. Arciero, A. Golombek, M.P. Hendrich, A.B. Hooper, Biochemistry 37 (1998) 523–529.
[18] M.P. Hendrich, D. Petasis, D.M. Arciero, A.B. Hooper, J. Am. Chem. Soc. 123 (2001) 2977–3005.
[19] I.V. Kurnikov, M.A. Ratner, A.A. Pacheco, Biochemistry 44 (2005) 1856–1863.
[20] J.H. Enemark, R.D. Feltham, Coord. Chem. Rev. 13 (1974) 339–406.
[21] M.P. Hendrich, A.K. Upadhyay, J. Riga, D.M. Arciero, A.B. Hooper, Biochemistry 41 (2002) 4603–4611.
[22] M.Z. Cabail, A.A. Pacheco, Inorg. Chem. 42 (2003) 270–272.
[23] M.Z. Cabail, J. Kostera, A.A. Pacheco, Inorg. Chem. 44 (2005) 225–231.
[24] M. Hoshino, M. Maeda, R. Konishi, H. Seki, P.C. Ford, J. Am. Chem. Soc. 118 (1996) 5702–5707.
[25] M. Hoshino, K. Ozawa, H. Seki, P.C. Ford, J. Am. Chem. Soc. 115 (1993) 9568–9575.
[26] V.S. Sharma, T.G. Traylor, R. Gardiner, H. Mizukami, Biochemistry 26 (1987) 3837–3843.
[27] E. Antonini, M. Brunori, J. Wyman, R.W. Noble, J. Biol. Chem. 241 (1966) 3236–3238.
[28] P.S.T. Yuen, D.L. Garbers, Ann. Rev. Neurosci. 15 (1992) 193–225.
[29] F.A. Walker, J. Inorg. Biochem. 99 (2005) 216–236.
[30] E.M. Maes, S.A. Roberts, A. Weichsel, W.R. Montfort, Biochemistry 44 (2005) 12690–12699.
[31] S.A. Roberts, A. Weichsel, Y. Qiu, J.A. Shelnutt, F.A. Walker, W.R. Montfort, Biochemistry 40 (2001) 11327–11337.
[32] M.O. Senge, Chem. Commun. (2006) 243–256.
[33] W. Jentzen, J.G. Ma, J.A. Shelnutt, Biophys. J. 74 (1998) 753–763.
[34] J.A. Shelnutt, X.Z. Song, J.G. Ma, S.L. Jia, W. Jentzen, C.J. Medforth, Chem. Soc Rev. 27 (1998) 31–41.
[35] W. Jentzen, X.Z. Song, J.A. Shelnutt, J. Phys. Chem. B 101 (1997) 1684–1699.
[36] D.M. Arciero, A.B. Hooper, FEBS Lett. 410 (1997) 457–460.
[37] D.J. Bergmann, A.B. Hooper, Eur. J. Biochem. 270 (2003) 1935–1941.
[38] B.O. Elmore, A.R. Pearson, C.M. Wilmot, A.B. Hooper, Acta Crystallograph. F Struct. Biol. Cryst. Commun. 62 (2006) 395–398.
[39] A.R. Pearson, B.O. Elmore, C. Yang, J.D. Ferrara, A.D. Hooper, C.M. Wilmot, Biochemistry 46 (2007) 8340–8349.
[40] J.M. Soler, E. Artacho, J. Gale, A. García, J. Junquera, P. Ordejón, D. Sánchez–Portal, J. Phys. Cond. Matt. 14 (2002) 2745–2779.
[41] S.E. Bari, M.A. Martí, V.T. Amorebieta, D.A. Estrin, F. Doctorovich, J. Am. Chem. Soc. 125 (2003) 15272–15273.
[42] N. Troullier, J.L. Martins, Phys. Rev. B 43 (1991) 1993–2006.
[43] S.G. Louie, S. Froyen, M.L. Cohen, Phys. Rev. B 26 (1982) 1738–1742.
[44] J.P. Perdew, K. Burke, M. Ernzerhof, Phys. Rev. Lett. 77 (1996) 3865–3868.
[45] L. Capece, M.A. Martí, A. Crespo, F.A. Doctorovich, D.A. Estrin, J. Am. Chem. Soc. 128 (2006) 12455–12461.
[46] M.A. Martí, A. Crespo, L. Capece, L. Boechi, D.E. Bikiel, D.A. Scherlis, D.A. Estrin, J. Inorg. Biochem. 100 (2006) 761–770.
[47] A. Ghosh, J. Biol. Inorg. Chem. 11 (2006) 712–724.
[48] D.A. Scherlis, D.A. Estrin, Int. J. Quantum. Chem. 87 (2002) 158–166.
[49] D.E. Bikiel, L. Boechi, A. Crespo, P.M. de Biase, S. Di Lella, M.C. Gonzalez Lebrero, M.A. Martí, A.D. Nadra, L.L. Perissinotti, D.A. Scherlis, D.A. Estrin, Phys. Chem. Chem. Phys. 8 (2006) 5611–5628.
[50] J. Wang, P. Cieplak, P.A. Kollman, J. Computat. Chem. 21 (2000) 1049–1074.
[51] W. Jentzen, M.C. Simpson, J.D. Hobbs, X. Song, T. Ema, N.Y. Nelson, C.J. Medforth, K.M. Smith, M. Veyrat, M. Mazzanti, R. Ramasseul, J.C. Marchon, T. Takeuchi, W.A. Goddard III, J.A. Shelnutt, J. Am. Chem. Soc. 117 (1995) 11085–11097.
[52] A. K Upadhyay, D.T. Petasis, D.M. Arciero, A.B. Hooper, M.P. Hendrich, J. Am. Chem. Soc. 125 (2003) 1738–1747.
[53] M.L. Quillin, R.M. Arduini, J.S. Olson, G.N. Phillips, J. Mol. Biol. 234 (1993) 140–155.
[54] W. Cao, J.F. Christian, P.M. Champion, F. Rosca, J.T. Sage, Biochemistry 40 (2001) 5728–5737.
[55] J.G. Ma, M. Laberge, X.Z. Song, W. Jentzen, S.L. Jia, J. Zhang, J.M. Vanderkooi, J.A. Shelnutt, Biochemistry 37 (1998) 5118–5128.
[56] L.D. Sparks, C.J. Medforth, M.S. Park, J.R. Chamberlain, M.R. Ondrias, M.O. Senge, K.M. Smith, J.A. Shelnutt, J. Am. Chem. Soc. 115 (1993) 581–592.
[57] A. Botulinski, J.W. Buchler, Y.J. Lee, R. Scheidt, M. Wicholas, Inorg. Chem. 27 (1988) 927–933.